

PAPER

Thermal-chemical instability of weakly ionized plasma in a reactive flow

To cite this article: Hongtao Zhong *et al* 2019 *J. Phys. D: Appl. Phys.* **52** 484001

View the [article online](#) for updates and enhancements.



IOP | ebooks™

Bringing you innovative digital publishing with leading voices to create your essential collection of books in STEM research.

Start exploring the [collection](#) - download the first chapter of every title for free.

Thermal-chemical instability of weakly ionized plasma in a reactive flow

Hongtao Zhong¹ , Mikhail N Shneider¹ , Mikhail S Mokrov² 
and Yiguang Ju¹

¹ Department of Mechanical and Aerospace Engineering, Princeton University, Princeton, NJ 08544, United States of America

² Institute for Problems in Mechanics, Russian Academy of Sciences, Moscow 119526, Russia

E-mail: hongtaoz@princeton.edu

Received 28 June 2019, revised 13 August 2019

Accepted for publication 21 August 2019


Published 11 September 2019



Abstract

The control of plasma instability of weakly ionized plasma in a reactive flow is of great importance in plasma-assisted combustion, catalysis, fuel reforming and material synthesis. In this work, we propose a new concept of plasma chemical instability and analyze the mechanisms and impact of plasma chemical instability on the transition from a uniform discharge to a contracted state of a self-sustained glow discharge in a reactive H₂-O₂-N₂ mixture. A one-dimensional numerical model for plasma chemical instability was developed which accounted for convective heat loss, Joule heating of plasma, and major non-equilibrium plasma-assisted combustion kinetic pathways including electron-impact ionization, vibrational energy transfer, electron attachment, combustion reactions, and heat release. The results showed that plasma chemical instability significantly modified the onset plasma current of plasma thermal instability. Specifically, the critical condition of the instability transition was strongly influenced by electron-impact reactant ionization, electron attachment to oxygen, endothermic/exothermic chemical reactions, and the formation of reaction products.

Keywords: plasma thermal instability, plasma chemical instability, weakly ionized plasma, reactive flow, hydrogen combustion

 Supplementary material for this article is available [online](#)

(Some figures may appear in colour only in the online journal)

1. Introduction

Weakly ionized plasma in a reactive flow has been widely used in plasma-assisted catalysis [1, 2], fuel reforming [3], chemical vapor deposition [4], and plasma-assisted combustion [5–7]. The homogeneous state of weakly ionized plasma, where plasma is distributed uniformly within a large volume, is one common plasma phenomenon seen in convective flow conditions. Another common plasma phenomenon is the contracted or constriction state, where inhomogeneous filaments are formed with much higher degree of ionization and local gas temperature. The transition from homogeneous plasma discharge to filamentary hot channels at sufficiently high currents is called plasma thermal-ionization instability or plasma thermal instability [8, 9].

Plasma thermal instability has been studied extensively in noble gases and air. The occurrence of plasma thermal instability is explained by the thermal-ionization mechanism [9]. For example, at isobaric conditions, a temperature perturbation from the local Joule heating induces thermal expansion, decreases the gas number density (N), and further increases the reduced electric field (E/N). Consequently, the ionization process controlled by the reduced electric field is amplified exponentially to trigger higher production rate of electrons and more intense heating. The positive feedback of the thermal-ionization mechanism is expressed as

$$T \uparrow \rightarrow N \downarrow \rightarrow E/N \uparrow \rightarrow T_e \uparrow \rightarrow \nu_i(T_e) \uparrow \rightarrow n_e \uparrow \rightarrow jE \uparrow \rightarrow T \uparrow. \quad (1)$$

Previous experimental studies [10] about plasma thermal instability were mostly conducted in a tube with diffusive or

convective cooling. It was observed that the discharge contracted non-uniformly: the contracted channel was formed in the vicinity of one electrode [11], then gradually grew toward the other electrode. Shneider *et al* developed two-dimensional modeling of the plasma thermal instability in nitrogen in a planar geometry [12] and in air in an axisymmetric cylindrical geometry [13]. The results showed that transition of the uniform plasma to the contracted state had a hysteresis cycle, which allowed the coexistence of both homogeneous and contracted states. By applying a sufficient perturbation, the volumetric plasma could abruptly transform into an unstable or contracted state. However, previous studies of plasma thermal instability were mostly limited to noble gases and air. How plasma instability would occur in reactive mixtures is not well understood.

In the reactive flow of weakly ionized plasma, with plasma-generated energetic electrons and reaction-generated active radicals and excited species, the plasma-enhanced decomposition and oxidation reactions will have strong kinetic effects on plasma instability. For instance, chemical reactions can release or absorb heat, which modify the system temperature, and further influence gas number density, reduced electric field, electron energy and electron number density. Chemical reactions can also change the mixture composition. As the ionization, attachment and other plasma kinetics vary greatly among different species, varying mixture composition brings more complexity. Therefore, in addition to the classical plasma thermal instability, the plasma-assisted chemical pathways may trigger a new plasma chemical instability (PCI) via a chemical kinetic mechanism. Unfortunately, to the authors' knowledge, few studies have been attempted to understand the plasma instability affected by chemical kinetics.

The objective of this work is to present a new concept of plasma chemical instability caused by chemical reactions. At first, a set of one-dimensional simplified self-consistent governing equations for the reactive flow of weakly ionized plasma is formulated. Then, numerical simulations are conducted to understand the couplings between plasma chemical instability and thermal instability in H₂-O₂-N₂ mixtures in the DC discharge. Several possible coupling mechanisms between plasma kinetics and combustion chemical kinetics for plasma thermal-chemical instability will be identified. Finally, the effect of critical parameters for the onset of plasma chemical instability will be discussed. The present analysis will advance the understanding of the kinetic and thermal interaction between plasma and chemical reactions and lay foundations for the future development of plasma-assisted aerospace propulsion systems as well as plasma-assisted processing and synthesis of chemicals and materials.

2. One-dimensional model for spatial-temporal dynamics of plasma chemical instability

Plasma instability is intrinsically three-dimensional due to the presence of the plasma-induced flow motion. As this work focuses on exploring the plasma chemical instability

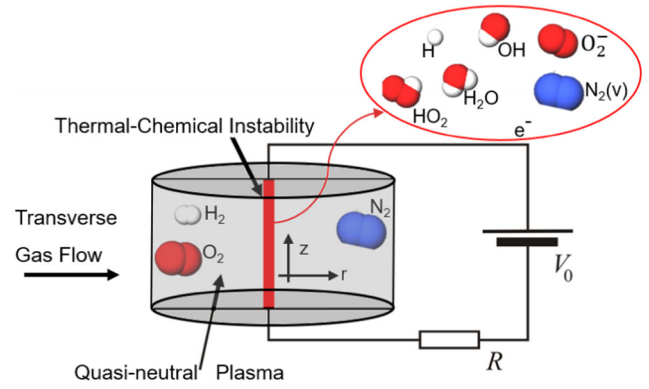


Figure 1. Schematic illustration of the computational domain for the plasma thermal-chemical instability in H₂-O₂-N₂ mixtures. The geometry is axisymmetric cylindrical. Some important combustion and plasma species are listed. Combustion chemical kinetics will influence the original thermal instability thermally and kinetically.

via the couplings between plasma and combustion chemical kinetics, we only analyze the instability in the initially homogeneous quasi-neutral axisymmetric positive column by using a simplified radial-dependent one-dimensional model [13] shown in figure 1. In the current analysis, the plasma sheath layers serve as the perturbation sources for the entire plasma volume [11].

The governing equations relate the densities of electrons, n_e , positive ions, n_+ , and negative ions, n_- , electric field, \mathbf{E} , translational gas temperature, T , and the vibrational temperature, T_v . The continuity equations for n_e , n_- , and n_+ are,

$$\frac{\partial n_e}{\partial t} - \frac{1}{r} \frac{\partial}{\partial r} \left[r(\mu_e n_e E_r + D_e \frac{\partial n_e}{\partial r}) \right] = Q_e \quad (2)$$

$$\frac{\partial n_-}{\partial t} - \frac{1}{r} \frac{\partial}{\partial r} [r(\mu_- n_- E_r)] = Q_- \quad (3)$$

$$\frac{\partial n_+}{\partial t} + \frac{1}{r} \frac{\partial}{\partial r} [r(\mu_+ n_+ E_r)] = Q_+ = Q_e + Q_- \quad (4)$$

Here Q_e , Q_- and Q_+ are source terms as $Q_e = (\nu_{ion} - \nu_a)n_e + \nu_d n_- - \beta_{e+} n_e n_+ - n_e/\tau$, $Q_- = \nu_a n_e - \nu_d n_- - \beta_{ii} n_- n_+ - n_-/\tau$. ν_{ion} , ν_a , ν_d are, respectively, ionization, attachment and detachment frequencies. β_{e+} and β_{ii} are the reaction coefficients for the electron-ion and ion-ion recombination. μ_e , μ_- and μ_+ are the mobilities for electrons and ions. D_e is the electron diffusion coefficient, and τ is the characteristic time for effective removal of charged particles and heat from the discharge due to the gas flow. The characteristic time τ is frequently introduced to simplify a multi-dimensional problem and make calculations more tractable (see [9]). Since we focus mainly on the instability mechanism, we follow this simplified representation for the transverse gas flow. As quasi-neutrality of the plasma is assumed, i.e. $n_+ = n_- + n_e$, it follows from equations 2–4 that

$$\frac{1}{r} \frac{\partial}{\partial r} \left[r(\mu_e n_e + \mu_- n_- + \mu_+ n_+) E_r + r D_e \frac{\partial n_e}{\partial r} \right] = 0 \quad (5)$$

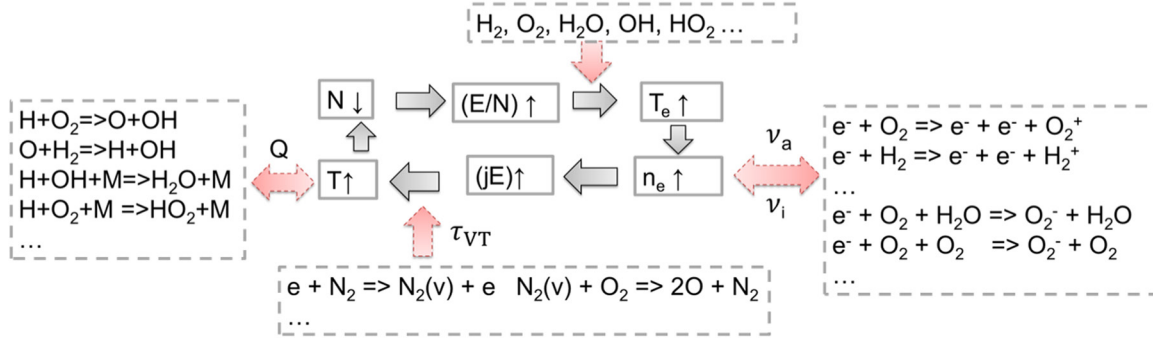


Figure 2. The schematic of the coupled plasma thermal-chemical mechanism in a plasma-assisted reactive flow. Black arrows (solid) refer to the original feedback in the plasma thermal instability. Red arrows (dotted) are some new couplings from the plasma chemical instability. Q is the heat absorption or heat release from chemical reactions. τ_{VT} refers to the timescale of the V–T relaxation process. ν_i and ν_a refer to plasma kinetic processes including ionization or attachment of combustion species.

from which the radial component of electric field, E_r , can be determined. The axial component, E_z , which is the bulk electric field between the two electrodes, can be calculated as

$$E_z = I / \int_0^{r_{max}} 2\pi r \sigma dr. \quad (6)$$

Here the discharge current, I , is determined by the external electric circuit. σ is the conductivity of the quasi-neutral plasma as $\sigma = e(\mu_e n_e + \mu_- n_- + \mu_+ n_+)$.

As the pressure is equalized quickly, we can assume that the gas is heated under isobaric conditions. By applying the ideal-gas law, the gas density, ρ , and temperature, T , are related as $\rho \propto T^{-1}$. The governing equation for the gas translational temperature is

$$\rho c_p \frac{\partial T}{\partial t} - \frac{1}{r} \frac{\partial}{\partial r} \left[r \left(\lambda \frac{\partial T}{\partial r} \right) \right] = Q_t \quad (7)$$

where $Q_t = \eta_j jE + (E_v - E_v^0)/\tau_{VT} + \hbar\omega\Pi - \rho c_p(T - T_0)/\tau + Q_c$, c_p is the specific heat of the mixture at the constant pressure; λ is the heat conductivity; η_j is the fraction of Joule heating (jE) responsible for the direct heating of the gas. Q_c accounts for the heat release or absorption during the plasma-assisted fuel pyrolysis and oxidation process, calculated as $Q_c = \sum_{j=1}^N H_j \dot{\omega}_j$. H_j is enthalpy of individual species while $\dot{\omega}_j$ is the rate of change of concentrations resulting from chemical reactions.

Another two terms from vibrational to translational (V–T) energy relaxation are also included, since a significant fraction of the deposited power in molecular discharges is pumped to the vibrational degrees of freedom and then released to translational degrees of freedom. $E_v^0(T_0)$ is the equilibrium value of E_v ; τ_{VT} is the V–T relaxation time; η_t is the fraction of Joule heat responsible for the translational excitation. $\hbar\omega\Pi$ accounts for the flow of vibrational quanta in the vibrational energy domain due to V–V energy relaxation. The calculation follows previous studies [12, 13]. The balance equation for vibrational energy, E_v , is

$$\frac{\partial E_v}{\partial t} - \frac{1}{r} \frac{\partial}{\partial r} \left[r \left(D \frac{\partial E_v}{\partial r} \right) \right] = Q_v \quad (8)$$

where $Q_v = -\hbar\omega\Pi - (E_v - E_v^0)/\tau_{VT} + \eta_v jE - (\rho/\rho_0)(E_v - E_v^0(T_0))/\tau$. D is the diffusion coefficient, η_v is the fraction of Joule heat responsible for the vibrational excitation. Combustion species are also updated by calling the CHEMKIN II package [14]. Equations (2)–(8) form the simplified governing equations for the plasma instability.

We use the symmetrical boundary conditions for the above system, i.e. $\partial n_e/\partial r = \partial n_-/\partial r = \partial T/\partial r = \partial E_v/\partial r = 0$ at the center ($r = 0$) and the edge of the domain ($r = r_{max}$). The set of equations is discretized by the finite volume method on the uniform grid ($r_{max} = 2$ cm). The grid size is 0.01 cm as it provides sufficient resolution of the instability phenomenon while reducing the computational time. To obtain the final time-invariant solutions, i.e. $\partial/\partial t = 0$ for major variables (densities of charge particles, the electric field, and translational gas temperature), the simulated time (t_{end}) exceeds 0.5 s for all the cases. Time steps range from 10^{-7} s to 10^{-6} s, which ensure the convergence and save on the computational resource.

3. Results and discussions

The dynamics of the above reactive plasma system is highly dependent on its source terms, which contain both plasma kinetics and chemical kinetics. Those reaction kinetics determined by the mixture composition, electron and gas temperatures create the couplings between plasma thermal instability and plasma chemical instability (shown in figure 2)

In the current work, we choose H_2 – O_2 – N_2 as the reactive mixture for two reasons. First, H_2 is a major fuel source and a key component for hydrocarbon heat release, which will potentially have impact on the classical plasma thermal instability. Second, the oxidation mechanism of H_2 is relatively small and well studied previously [15, 16], which allows for isolating specific species that play a major role in this process. In summary, understanding the plasma thermal-chemical instability in the H_2 – O_2 – N_2 system is a cornerstone for more complex fuel oxidation cases.

Two sets of conditions are mostly discussed, one at room temperature ($T_0 = 293$ K) and the other at a high ambient

Table 1. Reduced H₂-N₂-O₂ combustion kinetics [19]. Nine species and 20 reactions are considered. M is a third-body (see supplementary material for more details about plasma and combustion kinetics (stacks.iop.org/JPhysD/52/484001/mmedia)).

1	H + O ₂ → O + OH	2	O + H ₂ → H + OH
3	H ₂ + OH → H ₂ O + H	4	OH + OH → O + H ₂ O
5	H ₂ + M → H + H + M	6	O + O + M → O ₂ + M
7	H ₂ O + M → H + OH + M	8	O + H + M → OH + M
9	H ₂ O + H ₂ O → H + OH + H ₂ O	10	H + O ₂ + M → HO ₂ + M
11	HO ₂ + H → H ₂ + O ₂	12	HO ₂ + H → OH + OH
13	HO ₂ + O → O ₂ + OH	14	HO ₂ + OH → H ₂ O + O ₂
15	HO ₂ + HO ₂ → H ₂ O ₂ + O ₂	16	H ₂ O ₂ + M → OH + OH + M
17	H ₂ O ₂ + H → H ₂ O + OH	18	H ₂ O ₂ + H → HO ₂ + H ₂
19	H ₂ O ₂ + O → OH + HO ₂	20	H ₂ O ₂ + OH → HO ₂ + H ₂ O

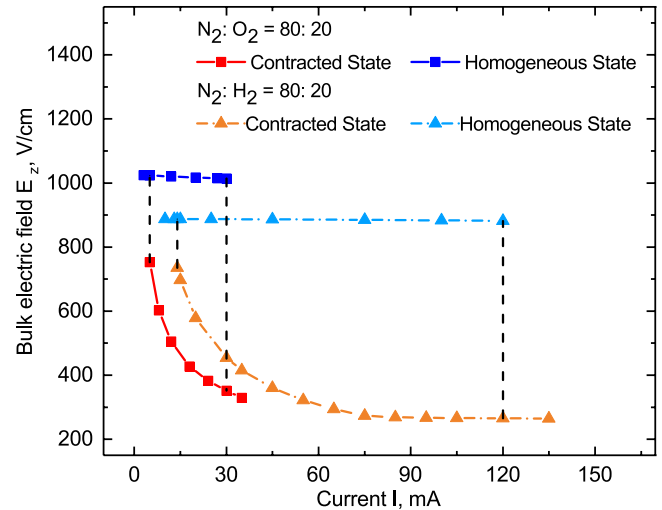
temperature ($T_0 = 800$ K). For the room temperature case, the pressure is set as 50 Torr and the convective time scale τ is 10^{-3} s. For the high temperature case, the pressure is raised to 250 Torr and the convective time scale $\tau = 10^{-2}$ s. We adjust those two values to keep the critical current I_{cr} in a reasonable range (10–100 mA). For all calculations, number densities of electrons, negative ions and positive ions are set to 10^{10} cm⁻³, 10^{10} cm⁻³, and 2×10^{10} cm⁻³. The initial molar fraction of N₂ is 0.8 and the equivalence ratio of H₂-O₂-N₂ mixtures is below unity. The selected values of pressures, temperatures and number densities of charged and neutral species result in the calculated reduced electric field between 10–80 Td and the calculated electron temperature between 0.8–1.5 eV, which can further simplify the kinetics involved in modeling the thermal-chemical instability.

For plasma kinetics, we consider direct electron-impact ionization, electron attachment and detachment, electron-ion and ion-ion recombination, and V-V and V-T energy relaxation related with major species as H₂, N₂, O₂ and H₂O. Other charged particles including OH⁻ and H⁺, produced either from intermediate radicals or dissociative plasma reactions, were ignored due to low concentrations of intermediate radicals and low energy input into the discharge during the whole process of plasma thermal-chemical instability. Electron attachment, detachment and the presence of negative ions are highly associated with electronegative gases in the mixture. Since in all the cases presented in this work the value of electron temperature does not exceed 0.8–1.5 eV for the entire range of E/N, we consider only the electron attachment in the three-body collisions as $e + O_2 + M \rightarrow O_2^- + M$ (M is a third-body). Although the vibrational-translational (V-T) energy relaxation time scales are different among species, in the H₂-O₂-N₂ mixture, we assume most vibrational energy is stored in the nitrogen molecules in view of rapid V-T relaxation of oxygen molecules [13]. The set of parameters are obtained via various literature [12, 13, 17, 18].

For combustion kinetics, we use the sub-mechanism for H₂-O₂-N₂ kinetics adapted from the well-validated HP Mech at Princeton [16, 19, 20], which includes 20 elementary reactions and nine species shown in table 1.

3.1. Effect of fuel pyrolysis

We first investigated the effect of plasma-assisted fuel pyrolysis on the onset of plasma instability by comparing the

**Figure 3.** Comparison of current-voltage characteristics with different compositions at $T_0 = 293$ K. (Squares correspond to N₂-O₂ and triangles correspond to N₂-H₂ mixtures.)

current-voltage characteristics $E = E(I)$ in N₂-O₂ and N₂-H₂ mixtures shown in figure 3. The hysteresis curve was calculated using the continuation method. For each branch of the curve, an initial point, either clearly homogeneous or clearly contracted, was chosen and the dynamics were simulated to obtain a stationary solution. Then the current was slightly increased or decreased, and the previous stationary solution was used as the initial condition to restart the simulation for a new current.

The top (blue) traces in figure 3 correspond to the uniform state of the volumetric plasma discharge while the bottom (red) symbols correspond to the contracted state after plasma instability. The vertical dashed lines represent the onset or transition limits between volumetric and contracted plasma states. Clearly, one can see a large shift of the critical current of the onset of plasma instability from the N₂-O₂ to N₂-H₂ system. The N₂-H₂ mixture system is more stable than the N₂-O₂ system. The higher ionization potential (H₂: 15.40 eV, O₂: 12.06 eV [21]) of H₂ and the endothermic H₂ decomposition reaction $H_2 + M \rightarrow H + H + M$ make it more difficult for the N₂-H₂ system to produce electrons and suppress the growth of the reduced electric field. The final distributions of the reduced electric field of the contracted states for two mixtures are also shown in figure 4. The presence of H₂ lowers

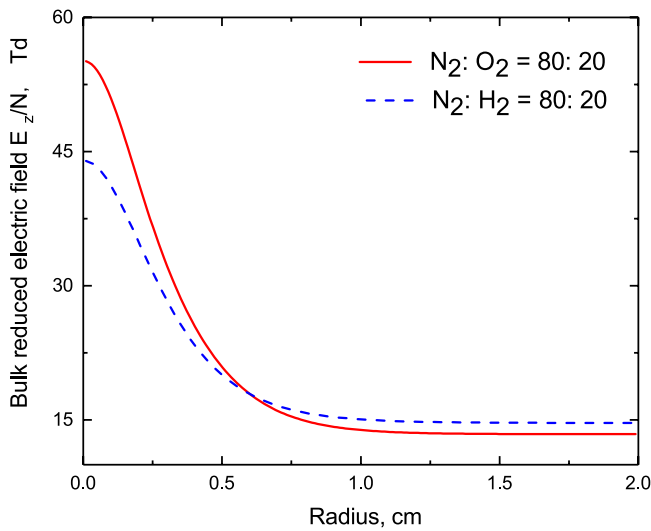


Figure 4. Comparison of the final distributions of reduced electric field (Td) of the contracted states for different compositions at $T_0 = 293$ K. $I = 35$ mA.

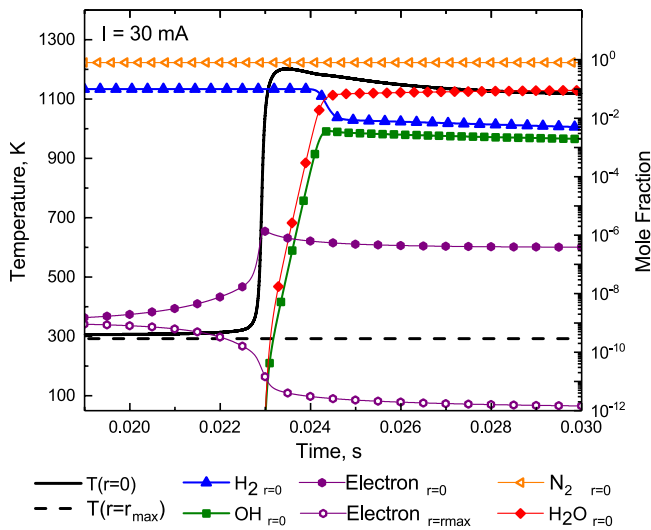


Figure 5. Time histories of key species and temperature at the center ($r = 0$) at 0.02 s–0.03 s at $T_0 = 293$ K.

the peak reduced electric field, which controls the plasma kinetics. As a result, the plasma combustion chemistry inhibits the plasma instability. Therefore, the increased fuel ionization potential and the endothermic fuel decomposition process is one mechanism of the plasma chemical instability.

3.2. Effect of exothermic fuel oxidation

Now we consider a $H_2-N_2-O_2$ system to examine the effect of fuel oxidation kinetics on the plasma instability at two different ambient temperatures as $T_0 = 293$ K and 800 K.

3.2.1. Case 1: $T_0 = 293$ K. First, we consider the process of combustion initiation in the hot contracted channel developed by plasma thermal instability. Time histories of temperature and species at the center of the computational domain ($r = 0$) are presented at figure 5. The initial mixture composition ratio was $H_2-O_2-N_2 = 80:10:10$ at room temperature

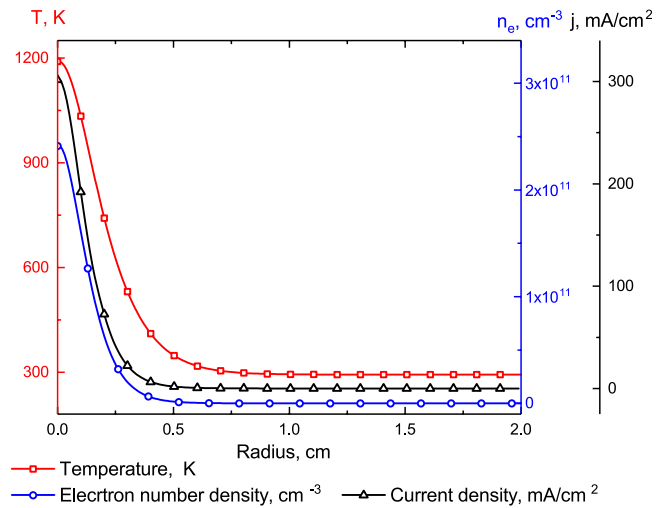


Figure 6. Final distributions of temperature, electron number density and current density of the contracted states at $T_0 = 293$ K.

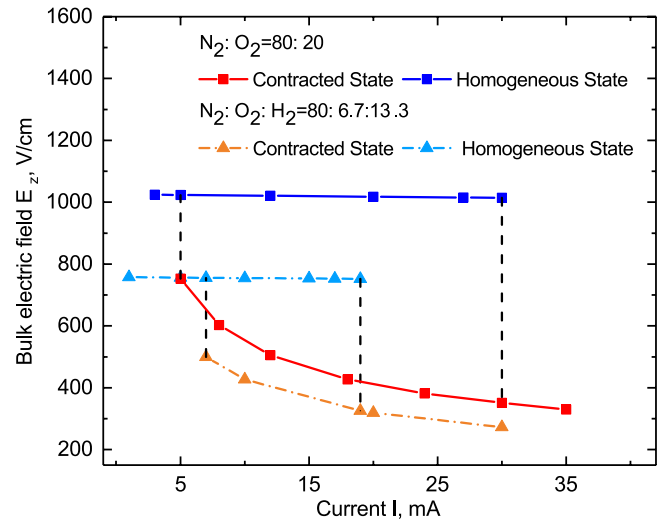


Figure 7. Comparison of current–voltage characteristics with and without fuel oxidation. Squares correspond to non-reacting N_2-O_2 mixtures, triangles correspond to $N_2-O_2-H_2$ mixtures. Initial composition is $N_2-O_2-H_2 = 80:6.7:13.3$. The $N_2-O_2-H_2$ flows continuously into the system with speed of 1.17×10^{-7} mol s^{-1} . $T_0 = 293$ K.

($T = 293$ K). The current is 30 mA. From figure 5, the thermal instability began with a sharp energy release and a rapid temperature increase from Joule heating and V–T energy relaxation within $\sim 10^{-3}$ s. The heat generated from plasma thermal instability raised the mixture temperature and decomposed fuel molecules and subsequently initiated combustion chemical kinetics. Combustion intermediates including OH and H were formed and the plasma-assisted ignition process occurred promptly within $\sim 10^{-2}$ s. The concentrations of intermediate species were decreased and the product such as H_2O gradually reached its chemical-equilibrium state. Several key reactions were involved in the plasma-assisted fuel oxidation process as $H + O_2 \rightarrow O + OH$ and $H + OH + M \rightarrow H_2O + M$. After chemical equilibrium was reached, there is no further effect from chemical kinetics on the plasma instability as the mixture was no longer reactive.

Table 2. Peak vibrational and translational temperature in 1D domain with or without fuel oxidation. Ambient temperature $T = 293$ K.

Mixture compositions	T , K	$I = 10$ mA	$I = 20$ mA	$I = 29$ mA
$N_2-O_2 = 80:20$	$T_{v,max}$	4365	5209	5688
	T_{max}	623	850	997
$N_2-O_2-H_2 = 80:6.7:13.3$	$T_{v,max}$	4428	5275	5765
	T_{max}	632	864	1018
$N_2-O_2-H_2 = 80:6.7:13.3$ (Set $Q_c = 0$)	$T_{v,max}$	4428	5256	5741
	T_{max}	632	854	1006

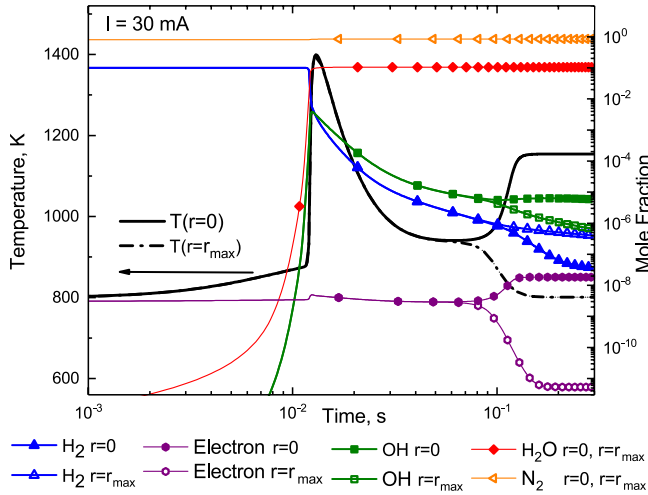


Figure 8. Time histories of key species and temperature at both ends ($r = 0$ and $r = r_{max}$). $T_0 = 800$ K.

The final distributions of electron number density, current density and temperature of the contracted states are shown in figure 6. Note that away from the center ($r = 0$), the mixture is too cold and no combustion reactions are activated.

The comparison of current–voltage characteristics between the non-reactive ($N_2-O_2 = 80:20$) and reactive mixture ($N_2-O_2-H_2 = 80:6.7:13.3$) in the same system is shown in figure 7. The lower branch represents the hot contracted channel. Since the combustion reactions release heat and change the mixture compositions, the system with plasma-assisted fuel oxidation becomes more unstable and the electron number density increases. Following equation (6), the bulk electric field E_z will decrease for the given current in the fuel oxidation case. The upper branch is the volumetric diffuse plasma discharge in which the plasma is maintained at room temperature homogeneously. Even though the chemical reaction at this low temperature is negligible, plasma chemical properties and the bulk electric field E_z still change due to different compositions. As a consequence, the critical current for the transition from the upper branch, i.e. homogeneous plasma state, to the lower branch, i.e. contracted plasma state is decreased and the resulting hysteresis region becomes more narrowed, indicating that chemical reactions in the hot contracted channel developed by plasma thermal instability makes the system more unstable.

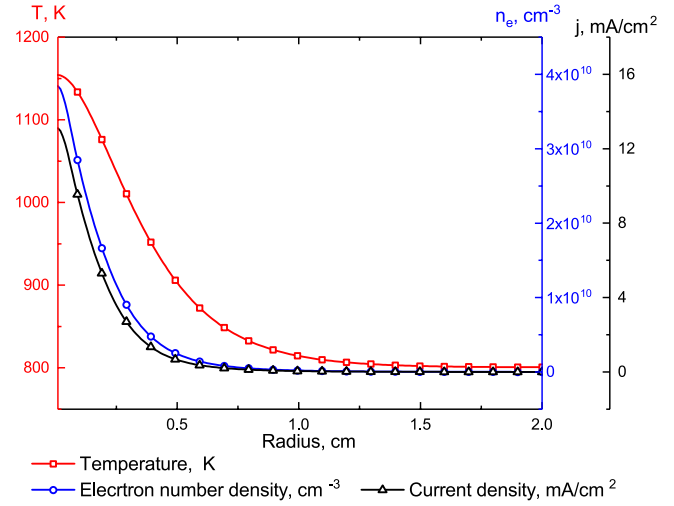


Figure 9. Final distributions of temperature, electron number density and current density. $T_0 = 800$ K.

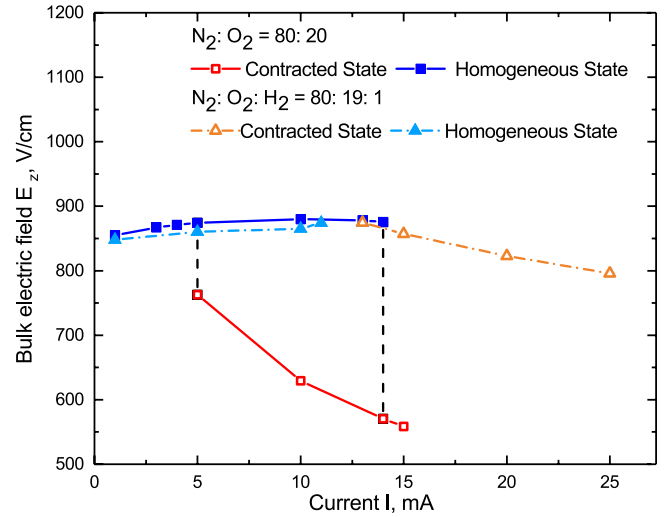


Figure 10. Comparison of current–voltage characteristics with and without fuel oxidation. Squares correspond to non-reacting N_2-O_2 mixtures, triangles correspond to $N_2-O_2-H_2$ mixtures (initial composition is $N_2-O_2-H_2 = 80:19:1$). Solid points correspond to the homogeneous state. Dotted points correspond to the contracted state. $T_0 = 800$ K.

Clearly combustion heat release can influence the stability boundary by increasing gas temperature and further increasing the reduced electric field. Moreover, the plasma-assisted fuel oxidation process changes the compositions and therefore the mixture plasma properties. To further evaluate the individual contribution from combustion heat release and the change of mixture properties by combustion, we run one extra case, where we artificially remove the combustion heat release by setting $Q_c = 0$. Even though the energy is not conserved for this case, the influence of combustion heat release on the final state can be observed and analyzed (shown in table 2).

From table 2, at a high current, i.e. a high temperature (over 1000 K), without considering the combustion heat release, there is a temperature drop from 1018 K to 1006 K.

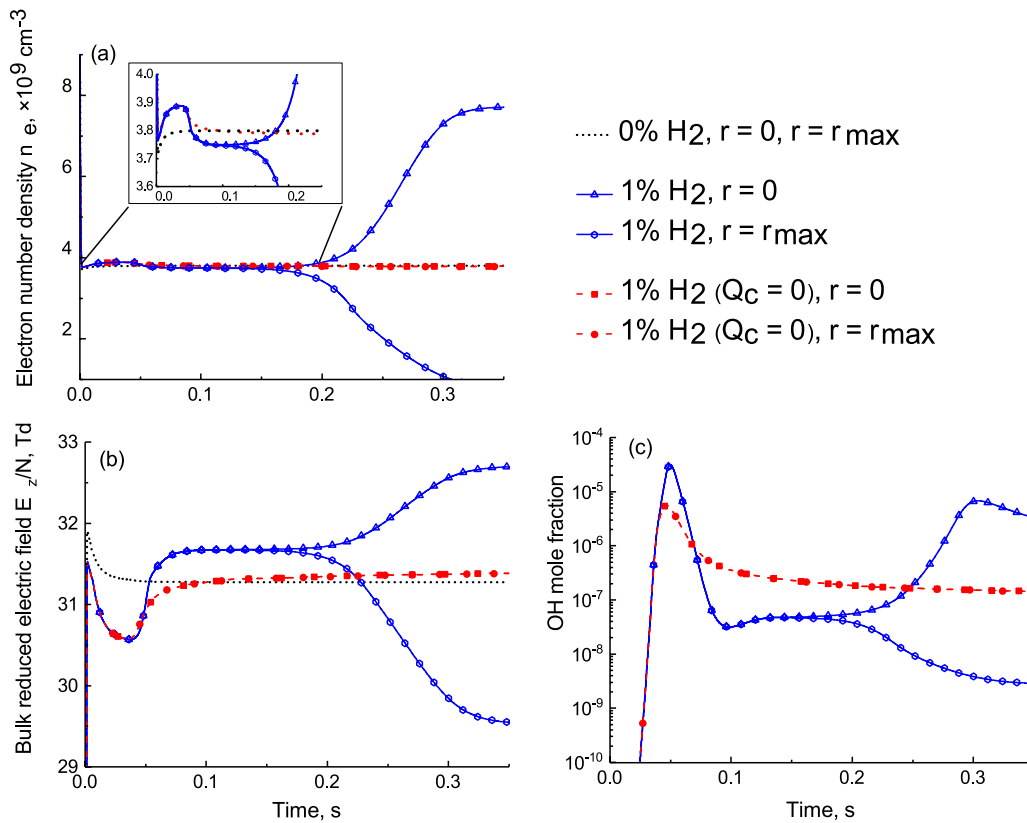


Figure 11. Comparison of time histories of (a) electron number density, (b) reduced electric field and (c) OH mole fractions at both ends ($r = 0$ and $r = r_{max}$) with and without fuel oxidation. Blue solid lines correspond to reacting mixtures. Red dash lines correspond to reacting mixtures without considering combustion heat release. The initial composition for both cases is N_2 - O_2 - $H_2 = 80:19:1$. Dotted lines correspond to the non-reacting mixture. $T_0 = 800$ K. $I = 13$ mA.

The peak vibrational temperature also decreases from 5765 K to 5741 K, indicating a lower degree of plasma non-equilibrium. However, at a low current, i.e. low temperature (lower than 800 K), the effect of combustion heat release on plasma properties from the H_2 - O_2 mixture is negligible. Nevertheless, the peak temperature in the oxidation case is still higher than the non-oxidation N_2 - O_2 mixture case, indicating that the change of mixture compositions due to fuel oxidation is the dominant mechanism for plasma chemical instability at low temperature.

3.2.2. Case 2: $T_0 = 800$ K. Preheating is a common approach to increase the system reactivity for various applications in combustion, fuel reforming and catalysis. To further demonstrate the chemical effect on the plasma instability, we preheat the mixture to 800 K, at which temperature the timescale of the combustion reactions may be comparable or shorter than the timescale for the formation of hot contracted channel by plasma thermal instability. In this case, it is combustion chemical kinetics that play the dominant role in triggering the instability.

The system dynamics are presented in figure 8. The initial composition is N_2 - O_2 - $H_2 = 80:10:10$. The current is $I = 30$ mA. The Joule heating first increased the temperature uniformly from 800 K. At $\sim 10^{-2}$ s chemical reactions were triggered homogeneously with a sharp temperature rise and composition change. At $\sim 10^{-1}$ s, the weakly ionized plasma

Table 3. Reaction rate coefficients of electron attachment to oxygen molecules at room temperature and different third body partners.

Three-body attachment to oxygen	Rate coefficient [22]
$e + O_2 + H_2 \rightarrow O_2^- + H_2$	$2.0 \times 10^{-31} \text{ cm}^6 \text{ s}^{-1}$
$e + O_2 + N_2 \rightarrow O_2^- + N_2$	$1.6 \times 10^{-31} \text{ cm}^6 \text{ s}^{-1}$
$e + O_2 + O_2 \rightarrow O_2^- + O_2$	$2.5 \times 10^{-30} \text{ cm}^6 \text{ s}^{-1}$
$e + O_2 + H_2O \rightarrow O_2^- + H_2O$	$1.4 \times 10^{-29} \text{ cm}^6 \text{ s}^{-1}$

began to transit from a homogeneous state to a contracted state. N_2 was the major non-reactive species. The mole fraction of N_2 varied from 0.8 to around 0.85 during the whole process, while the mole fractions of highly-reactive electrons and combustion radicals increased sharply for orders of magnitude. The above discussion clearly shows the multi-scale nature of the plasma thermal-chemical instability. Nonuniform distributions of electron number density, current density and electric field are observed in the radial direction when time exceeds 0.3 s (shown in figure 9). However, unlike the case where combustion is triggered only after the contracted channel is developed by plasma thermal instability, in the present case, chemical reactions happen in the whole domain and the development of plasma instability is dominated by the thermal-chemical effects from combustion kinetics.

The critical current for plasma instability is also decreased compared with the air case at the ambient temperature of 800 K. As shown in figure 10, the presence of

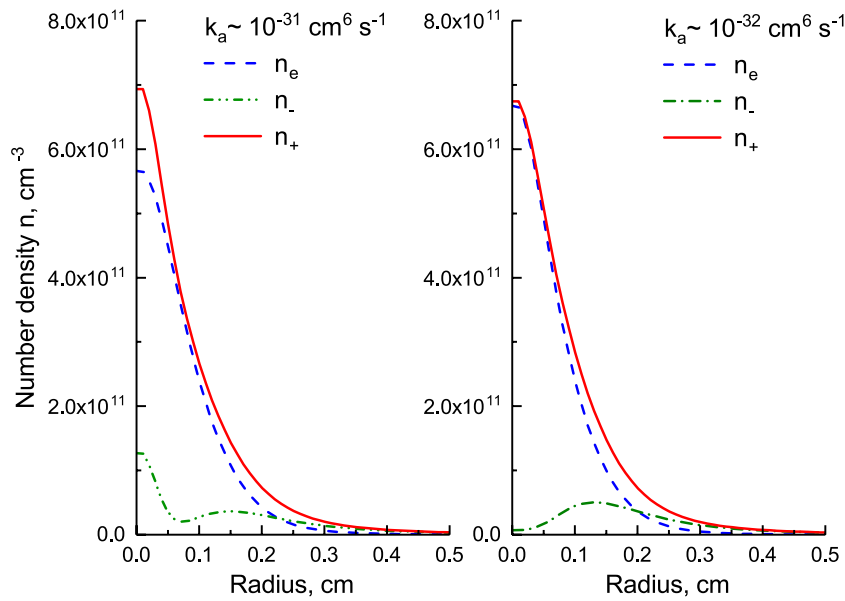


Figure 12. Comparison of the final distribution of charge particles of the contracted states for $k_a \sim 10^{-31} \text{ cm}^6 \text{ s}^{-1}$ and $k_a \sim 10^{-32} \text{ cm}^6 \text{ s}^{-1}$. $I = 30 \text{ mA}$. $T_0 = 293 \text{ K}$.

only one percent hydrogen shifts the critical current from $I = 14 \text{ mA}$ to $I = 11 \text{ mA}$. The classical hysteresis curve for non-reacting case is degenerated into a single-valued curve in the reacting case, indicating that the contracted state can sustain at high electric field. To explain this, we compare the evolution of electron number density, reduced electric field, and OH mole fractions at both ends in reacting and non-reacting cases at the same condition (shown in figure 11). From figure 11, we find that combustion heat release triggers the plasma chemical instability at high ambient temperature. Firstly, the combustion heat release accelerates the chemical reaction rates. As a result, combustible mixtures react more promptly into products (see figure 11(c)) and the plasma chemical properties change rapidly during the reaction process. Secondly, combustion heat raises the temperature, thus increases the reduced electric field (E/N) (see figure 11(b)) and therefore increase the ionization rates. More importantly, the temperature rise increases the specific volume and directly reduces electron and species number density (see figure 11(a)). Therefore, the plasma conductivity σ decreases and the bulk electric field E_z can be maintained at a high level (see equation (6)) in the case of plasma chemical instability. It should be pointed out that if we artificially set the combustion heat release term $Q_c = 0$ in the modeling, then combustion products are formed more slowly and the reduced electric field and electron number density gradually reach the similar levels as those of the homogeneous air plasma case. In that case, the homogeneous state can be maintained and no plasma contraction is observed for the initial $\sim 0.3 \text{ s}$.

To summarize, the exothermic fuel oxidation not only affects the final contracted state of plasma instability, but also modifies the initiation of plasma instability. In addition to Joule heating, combustion heat release and combustion chemical kinetics play an important role in the plasma chemical instability.

3.3. Effect of electron attachment

Electron attachment is another key kinetic process in plasma chemical instability. Combustion mixtures typically have higher concentrations of water and oxygen. As shown in table 3, the rate coefficients of attachment reactions for O_2 and H_2O is more than one order of magnitude higher than those for N_2 . As a consequence, reactive mixtures may have a higher attachment rate by orders of magnitude compared with air or other diluents.

To explore the influence of high attachment rate on the plasma instability, we artificially perturb the overall attachment rate in the $\text{N}_2\text{-O}_2$ mixture. The different distributions of charged particles at the contracted state are shown in figure 12. With a higher attachment rate, more electrons were attached to molecules, yielding a higher population of negative ions. When the plasma chemical instability was triggered, the increase of negative ions and decrease of electron number density reduced the overall charge particle mobility and thus stabilized the system. Therefore, high electron attachment rate to oxygen and water will suppress the electron production and plasma chemical instability. With the increase of oxygen concentration in a reactive mixture, there is a competition between plasma-assisted heat release and electron attachment to oxygen in PCI. Higher oxygen concentrations lead to strong electron attachment, which stabilizes PCI. Meanwhile, higher oxygen content also enhances the oxidation process, which would promote radical production and heat release processes, resulting in destabilization of the system.

4. Conclusion

A new concept of PCI caused by coupled plasma-combustion chemistry is presented and analyzed in a reactive flow of weakly ionized plasma. The results show that the plasma chemical instability affects the critical plasma current for the

transition between the homogeneous state and the contracted state originally triggered by the plasma thermal instability. The plasma chemical instability can couple with the plasma thermal instability via the endothermic and exothermic plasma-assisted combustion reactions by changing the local temperature. Moreover, the electron attachment to oxygen and combustion products as well as the change of plasma properties by chemical reactions also contribute to the plasma chemical instability without plasma-assisted reaction heat release. Specifically, the results reveal that the endothermic electron-impact fuel dissociation and excitation reactions and electron attachment processes will increase the plasma stability. Moreover, plasma-assisted combustion heat release will promote the plasma instability. Understanding the impact of chemical reaction kinetics on plasma instability will open more new applications for efficient ignition and material synthesis. Future modeling with detailed chemical kinetics is necessary for quantitative studies of plasma chemical instability with strong non-equilibrium of plasma energy distributions at high electric field strength.

Acknowledgments

This work was supported by the US National Science Foundation (NSF) Grant on plasma instability (No. CBET-1903362) and the US Department of Energy (DOE) Grant of Plasma Science Center. Mikhail S Mokrov's research was supported in part by the Russian Science Foundation (RSF) Grant 16-11-10275. We thank Dr Shuqun Wu for helpful discussions in stability analysis of PCI. We also thank Mr Xingqian Mao, Timothy Chen, and Aric Rouso for the insightful discussions of plasma-assisted combustion kinetics.

ORCID iDs

Hongtao Zhong  <https://orcid.org/0000-0003-4064-6298>
 Mikhail N Shneider  <https://orcid.org/0000-0002-2925-7008>
 Mikhail S Mokrov  <https://orcid.org/0000-0002-0712-5135>

References

- [1] Whitehead J C 2016 Plasma-catalysis: the known knowns, the known unknowns and the unknown unknowns *J. Phys. D: Appl. Phys.* **49** 243001
- [2] Chu W, Wang L, Chernavskii P A and Khodakov A Y 2008 Glow-discharge plasma-assisted design of cobalt catalysts for Fischer–Tropsch synthesis *Angew. Chem., Int. Ed.* **47** 5052–5
- [3] Gutsol A, Rabinovich A and Fridman A 2011 Combustion-assisted plasma in fuel conversion *J. Phys. D: Appl. Phys.* **44** 274001
- [4] Silva F, Hassouni K, Bonnin X and Gicquel A 2009 Microwave engineering of plasma-assisted CVD reactors for diamond deposition *J. Phys.: Condens. Matter* **21** 364202
- [5] Starikovskaia S M 2006 Plasma assisted ignition and combustion *J. Phys. D: Appl. Phys.* **39** R265
- [6] Starikovskaia S M 2014 Plasma-assisted ignition and combustion: nanosecond discharges and development of kinetic mechanisms *J. Phys. D: Appl. Phys.* **47** 353001
- [7] Ju Y and Sun W 2015 Plasma assisted combustion: dynamics and chemistry *Prog. Energy Combust. Sci.* **48** 21–83
- [8] Velikhov E P, Golubev V S and Pashkin S V 1982 Glow discharge in a gas flow *Sov. Phys.—Usp.* **25** 340
- [9] Raizer Y P 1991 Gas discharge physics
- [10] Eletskaia A V and Smirnov B M 1996 Nonuniform gas discharge plasma *Phys.—Usp.* **39** 1137
- [11] Akishev Y, Karalnik V, Kochetov I, Napartovich A and Trushkin N 2014 High-current cathode and anode spots in gas discharges at moderate and elevated pressures *Plasma Sources Sci. Technol.* **23** 054013
- [12] Shneider M N, Mokrov M S and Milikh G M 2012 Dynamic contraction of the positive column of a self-sustained glow discharge in molecular gas *Phys. Plasmas* **19** 033512
- [13] Shneider M N, Mokrov M S and Milikh G M 2014 Dynamic contraction of the positive column of a self-sustained glow discharge in air flow *Phys. Plasmas* **21** 032122
- [14] Kee R J, Rupley F M and Miller J A 1989 Chemkin-II: a Fortran chemical kinetics package for the analysis of gas-phase chemical kinetics *Technical Report* Sandia National Labs., Livermore, CA
- [15] Law C K 2010 *Combustion Physics* (Cambridge: Cambridge University Press) (<https://doi.org/10.1017/CBO9780511754517>)
- [16] Burke M P, Chaos M, Ju Y, Dryer F L and Klippenstein S J 2012 Comprehensive H₂/O₂ kinetic model for high-pressure combustion *Int. J. Chem. Kinetics* **44** 444–74
- [17] Phelps A V 1998 Electron transport data *Data Compilation*
- [18] Aleksandrov N L 1988 Three-body electron attachment to a molecule *Sov. Phys.—Usp.* **31** 101
- [19] Santner J, Dryer F L and Ju Y 2013 The effects of water dilution on hydrogen, syngas, and ethylene flames at elevated pressure *Proc. Combust. Inst.* **34** 719–26
- [20] Yang S, Yang X, Wu F, Ju Y and Law C K 2017 Laminar flame speeds and kinetic modeling of H₂/O₂/diluent mixtures at sub-atmospheric and elevated pressures *Proc. Combust. Inst.* **36** 491–8
- [21] Watanabe K 1957 Ionization potentials of some molecules *Chem. Phys.* **26** 542–7
- [22] Fridman A 2008 *Plasma Chemistry* (Cambridge: Cambridge University Press) (<https://doi.org/10.1017/CBO9780511546075>)